J. Fluid Mech. (1986), *vol.* 163, *pp.* 459–478
Printed in Great Britain

Simultaneous flow visualization and Reynolds-stress measurement in a turbulent boundary layer

By A. M. TALMON, J. M. G. KUNEN AND G. OOMS
Delft University of Technology, Laboratory for Aerodynamics and Hydrodynamics, Delft, The Netherlands

(Received 9 November 1984 and in revised form 30 September 1985)

Flow visualization and Reynolds-stress measurement were combined in an investigation of a turbulent boundary layer in a water channel. Hydrogen bubbles were used to visualize the flow; a laser-Doppler anemometer capable of measuring two velocity components was applied to measure the instantaneous value of the Reynolds stress. Owing to the three-dimensional, time-dependent character of the flow it was rather difficult to identify flow structures from measured velocity signals, especially at larger distances from the wall. Despite this difficulty a method based on the instantaneous value of the Reynolds stress could be developed for detecting bursts in the wall region of the boundary layer. By this method the three-dimensional, time-dependent character of the flow is taken into account by attributing to the same burst ejections occurring successively with very short time intervals. This identification procedure is based on a comparison on a one-to-one basis between visualized flow structures and measured values of the Reynolds stress. The detected bursts were found to make a considerable contribution to the momentum transport in the boundary layer.

1. Introduction

Flow visualization has revealed the existence of coherent structures in turbulent boundary layers. However, the description of a coherent structure is too qualitative when based on flow visualization alone. Consequently efforts have been made to obtain quantitative data on coherent structures by simultaneous flow visualization and measurement of the velocity field.

As is stated in many papers, coherent structures in boundary layers are important for transport processes, so it is interesting to relate visualized structures to instantaneous values of the Reynolds stress. For this reason the flow in the turbulent boundary layer in an open, recirculating water channel was visualized by means of hydrogen bubbles. The visualized flow was filmed, while simultaneously the instantaneous Reynolds stress was measured by means of a laser-Doppler anemometer capable of measuring two velocity components, and the results were compared.

Simultaneous experiments, using two-component measuring systems, have been performed by Offen & Kline (1973), Falco (1977) and Bogard (1982). Falco's experiments were carried out in the outer region of the boundary layer, whereas Offen & Kline's and Bogard's experiments were performed in the wall region. Falco used smoke while Offen & Kline and Bogard used dye to visualize low-speed streaks and the bursting process.

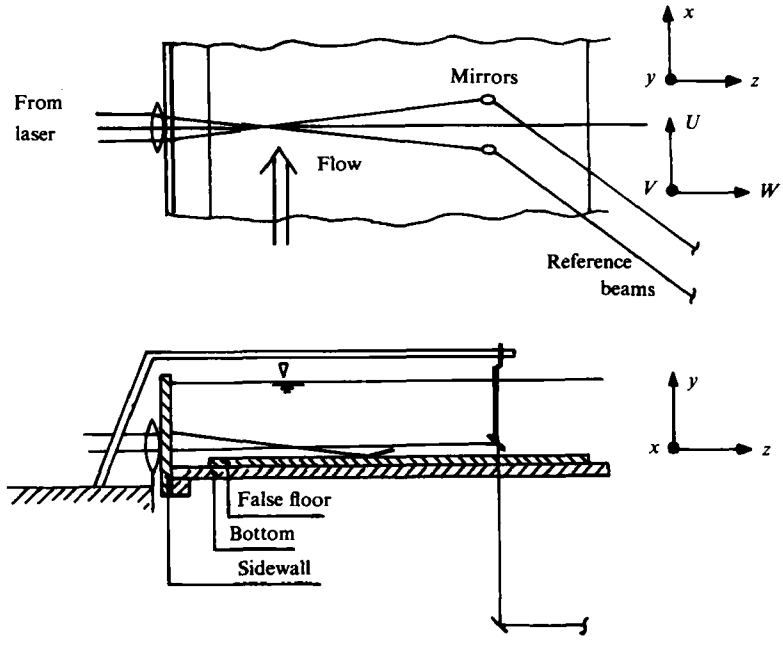

FIGURE 1. Laser-Doppler arrangement in channel.

Our experiments were rather similar to Bogard's. However, by using hydrogen bubbles and a laser-Doppler anemometer, we were able to measure close to the wall in the wall region without disturbing the flow downstream. This is an important feature because it enabled us to study visually the development of structures already measured. In this paper our results will be compared with those of Bogard.

In §2 the experimental set-up is described, in §3 some experimental results for the velocity field are given, in §4 the observed structures are reported and in §5 the relation between observed flow structures and the Reynolds stress is discussed.

2. Experimental set-up

An open, recirculating water channel was employed. Water from a supply vessel was pumped by a centrifugal pump into a constant-pressure tank. By means of overflows the water could flow from there through an open settling chamber (with corner-vanes and a flow straightener, contraction ratio of 5:1 at a water depth of 9 cm) and an open channel (dimensions $280 \times 150 \times 12$ cm^3) back into the supply vessel. On the bottom of the channel a false floor (dimensions $210 \times 50 \times 1.6$ cm^3) was placed at 5.4 cm from the left sidewall of the channel (see figure 1). In that way visualization could be performed without disturbing the flow or damaging the channel bottom, as small holes could be drilled in the false floor for fixing the visualization wires. Transition from laminar to turbulent flow was fixed at 9 cm downstream of the channel entrance by means of a trip wire with a diameter of 3 mm. An adjustable threshold was installed 245 cm downstream of the entrance to ensure a certain water depth. The water speed between the constant-pressure tank and the settling chamber, and between the channel and the supply vessel, could be adjusted with valves. The channel bottom and the false floor were made of glass and the sidewalls of Perspex.

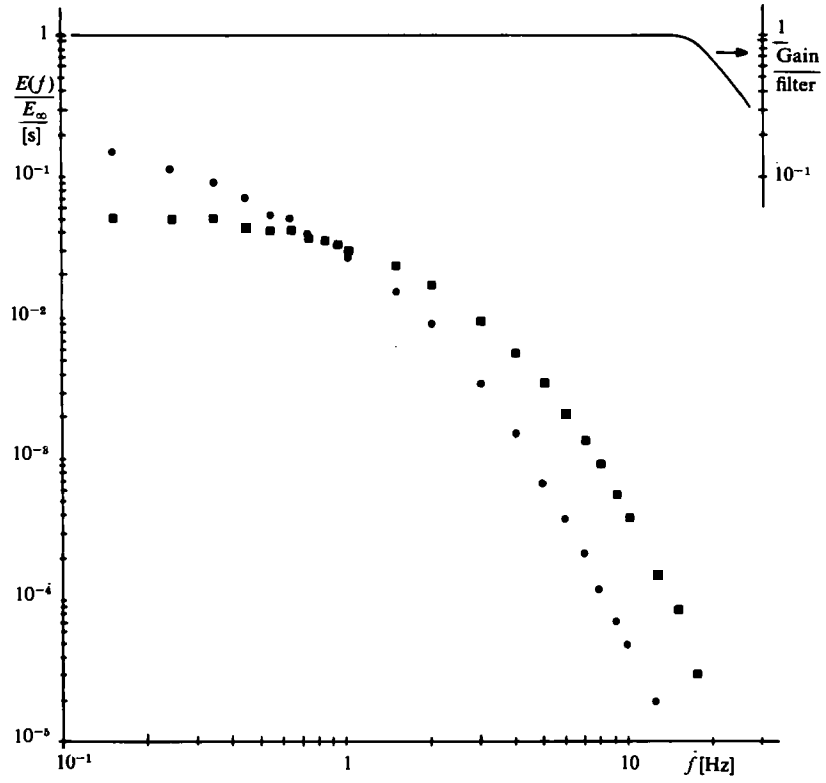

FIGURE 2. Energy spectra measured in channel flow. $Re_\theta = 730$; $y^+ = 14.3$; ●, u; ■, v.

The settling chamber and the channel were mounted so as to be free of vibrations from the rest of the system.

Laser-Doppler anemometer measurements were performed in the turbulent boundary layer along the false floor 158 cm downstream of the trip wire and 13.4 cm from the sidewall where the laser was mounted (see figure 1).

The anemometer was operated in the reference-beam mode and was capable of measuring instantaneously two mutually perpendicular velocity components. The two velocity components U and V, respectively the main-flow velocity component and the velocity component normal to the wall (see figure 1), were not measured directly; however, at an angle of 45° the sum and difference of these components were measured. The measurements were performed with a 6 mW He–Ne laser. To create the main beam and the reference beams and to provide for the necessary preshift a rotating diffraction grating was used (rotation frequency 49.7 Hz, preshift frequency 815 kHz). With a lens ($f = 120$ mm) the three beams were focused onto one point: the measuring volume (dimensions 0.65×0.06 mm^2). Because the channel was too wide to pick up the reference beams at the other side of the channel (too much light was scattered), two small mirrors were placed in the channel 43 cm from the sidewall to deflect the two reference beams down through false floor and channel bottom (see figure 1). Beneath the channel two other mirrors deflected the beams to the photodetectors. The total measuring system could be translated vertically.

Before recording on a magnetic disc the fluctuating tracer output signals were low-pass filtered, cutoff frequency 20 Hz, to remove the rotation frequency of the rotating grating. The choice of this cutoff frequency is acceptable, as can be seen in

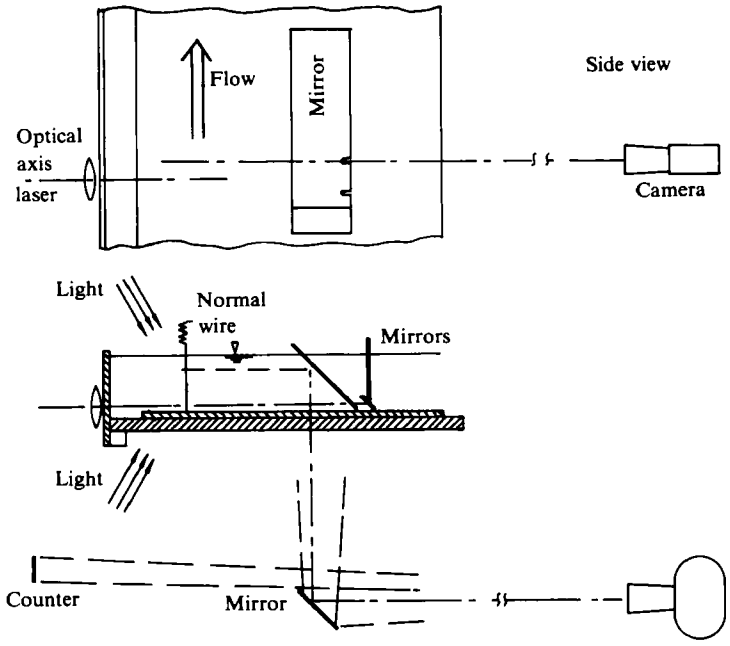

FIGURE 3. Arrangement for filming the channel flow in side view.

figure 2, in which the measured one-dimensional spectra and filter characteristic are shown. The measurements in the turbulent boundary layer were performed with sampling rates of 50 and 100 Hz (to avoid aliasing in spectrum calculations) and with a duration of 30 min. With a minicomputer the turbulence intensities u' and v', the skewness and flatness of u- and v-fluctuations (S_u, S_v, F_u and F_v) and the Reynolds stress $-\rho\overline{uv}$ were computed. The mean velocity $\overline{U}$ was calculated from the directly measured v.c.o.-frequency (voltage controlled oscillator) of the tracker. The v.c.o.-frequency equals the sum of Doppler, preshift and intermediate frequency.

The hydrogen-bubble technique was adopted to visualize the flow. In this technique a fine platinum wire is stretched in the water and is the negative electrode of a d.c. circuit. Hydrogen bubbles are generated at the wire when the circuit is electrified. These bubbles are the markers for flow visualization. By pulsing the voltage at regular time intervals bubble lines are produced. On a single photograph the shapes of the bubble lines indicate the integrated effect of the velocities experienced by the bubbles since their release from the wire. The position and timing of a particular type of flow structure can be determined by comparing lines' movements at successive frames of a square. In the channel wires were placed in normal (y) and transverse (z) directions to visualize (x, y)- and (x, z)-planes of the flow (see figures 3 and 4). The wires used were 0.07 mm in diameter. The normal wire was 9 cm in length and the total transverse wire 28.5 cm long, of which 11.5 cm was not insulated. The normal wire was tightly fitted into a small hole drilled in the false floor 38 mm upstream of the measuring station of the laser-Doppler anemometer. The transverse wire was soldered to supports which could be translated vertically 9.3 mm upstream of the measuring station. The voltage applied to the wires was pulsed with a frequency of 20 Hz.

Simultaneously, flow visualization with hydrogen bubbles and measurements with the laser-Doppler anemometer were performed. The measured fluctuating tracker

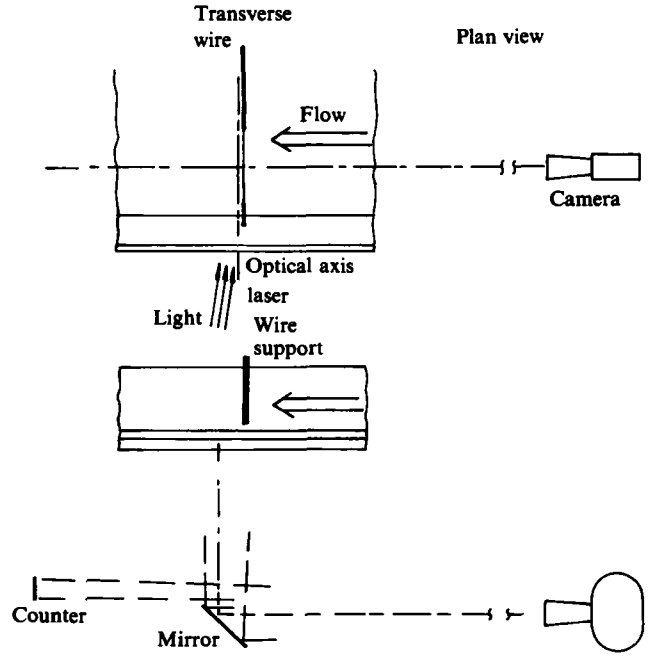

FIGURE 4. Arrangement for filming the channel flow in plan view.

output signals were recorded on magnetic disc and the visualized flow was filmed with an 11 mm camera. A much more detailed description of the experimental set-up with which the simultaneous experiments were performed can be found in Kunen (1984) and Talmon (1984).

The flow was filmed in side view ((x, y)-plane) and in plan view ((x, z)-plane). In plan view the camera field of view was 70×110 mm^2 (in the streamwise and transverse directions respectively). In plan view it was impossible to film and measure at the same distance from the wall, because too much laser light was scattered by the hydrogen-bubble plane. It appeared necessary to separate the measuring point and the platinum wire over 2 mm in a normal direction. The side-view dimensions of the camera field of view were 143×68 mm (in streamwise and normal direction respectively). The clock pulse, that the minicomputer used for sampling, was also used to link the recorded velocity components with the corresponding film frames. The clock pulse actuated a counter which appeared at the top of each frame, so the numbers on the frames correspond to the time series of the recorded signals. Because the camera magazine could contain films of 30 m maximum length and because filming was performed with about 45 frames/s, the flow could only be filmed during approximately the first 90 s of sampling. The exposure time was $\frac{1}{125}$ s, so relatively sharp photographs could be taken. To be able to compare flow patterns and measured signals the position of the measuring point must be visible on the frames. When filming in side view the laser beams show that position but, because in plan view the measurements were performed approximately 2 mm below the visualized 'plane', the position of the measuring point had to be indicated on the frames before or after filming. Therefore the first metre of each film was exposed with the platinum wire at the same distance from the wall as the reference beams. Then the hydrogen bubbles were generated continuously. Thus the position of the intersection of the laser beams, the measuring volume, was marked on each film.

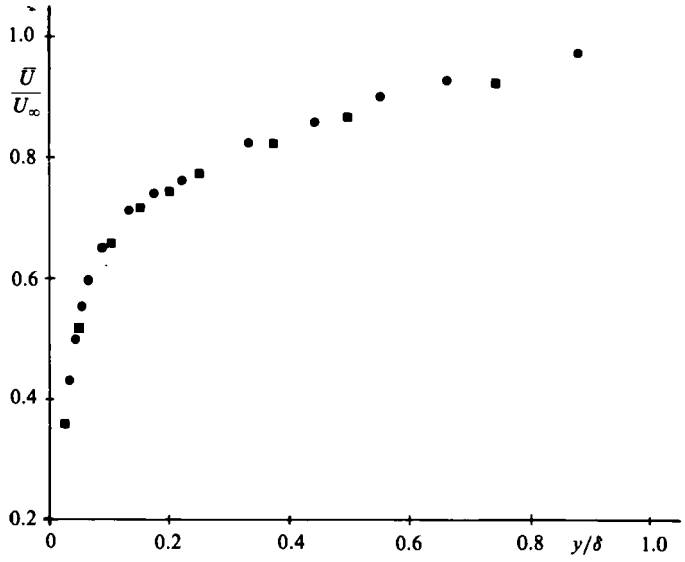

FIGURE 5. Time-mean-velocity distribution in channel flow. ●, $Re_\theta = 770$; ■, 730.

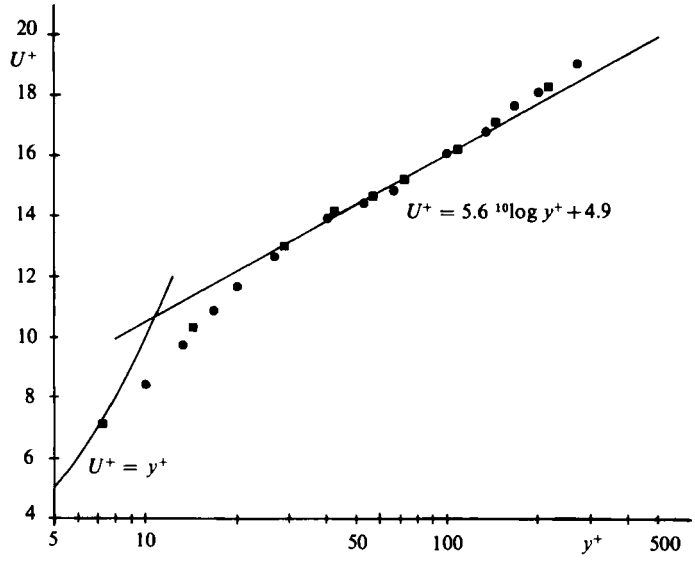

FIGURE 6. Logarithmic time-mean-velocity distribution in channel flow. Symbols as in figure 5.

3. Experimental results

Traverses were made with the laser-Doppler anemometer to study the turbulent boundary layer that had developed over the false floor. The free-stream water speed was 14.1 and 13.4 cm/s and the water depth was about 9 cm. In figures 5 and 6 the measured mean-velocity distributions are shown. The displacement thickness δ^* and the momentum thickness θ were calculated by numerical integration. Using the empirical velocity distribution $\bar{U}/U_\infty = (y/\delta)^{1/n}$ the boundary-layer thickness δ was computed; see Hinze (1975). The wall-friction velocity u_τ was derived by fitting the velocity data to Clauser's form of the logarithmic law; see Clauser (1956). In table 1

U_∞ (cm/s)	u_τ (mm/s)	δ (mm)	δ^* (mm)	θ (mm)	Re_θ
14.1	7.2	45.6	8.9	5.9	770
13.4	6.8	40.6	7.5	5.2	730

TABLE 1. Channel-flow parameters

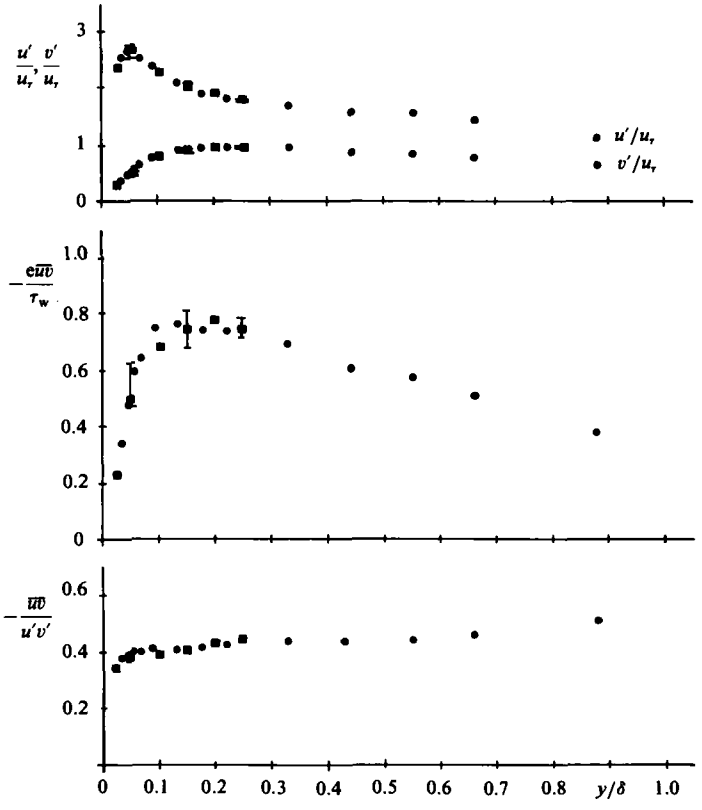

FIGURE 7. Distribution of turbulence quantities in channel flow. ●, $Re_\theta = 770$; ■, 730; ■, 730 (films).

the channel-flow parameters are summarized and in figure 7 the distributions of the turbulence intensities u' and v', the Reynolds stress in dimensionless form, and the correlation factor are shown. Also indicated are the maximum and minimum values of the Reynolds stress of the 30 min signals measured during and after filming. Eight side-view films were exposed with velocity measurements at dimensionless distance to the wall of $y^+ = 14$, 43 and 72. Four plan-view films were exposed with measurements at $y^+ = 14$ and 43. The flow conditions during filming were approximately the same as during the second traverse (table 1, $U_\infty = 13.4$ cm/s). The scatter in these results, see figure 7, could be caused by the hydrogen bubbles which are rising slowly through buoyancy. The distributions of u'/u_τ, S_u and F_u and of v'/u_τ, S_v and F_v are given on a logarithmic scale in figures 8 and 9 respectivcly. Comparison with the measurements of Gupta & Kaplan (1972) in a turbulent boundary layer and of Kreplin & Eckelmann (1979) in a turbulent channel flow yields a good agreement for the wall region. The agreement is less good in the outer region

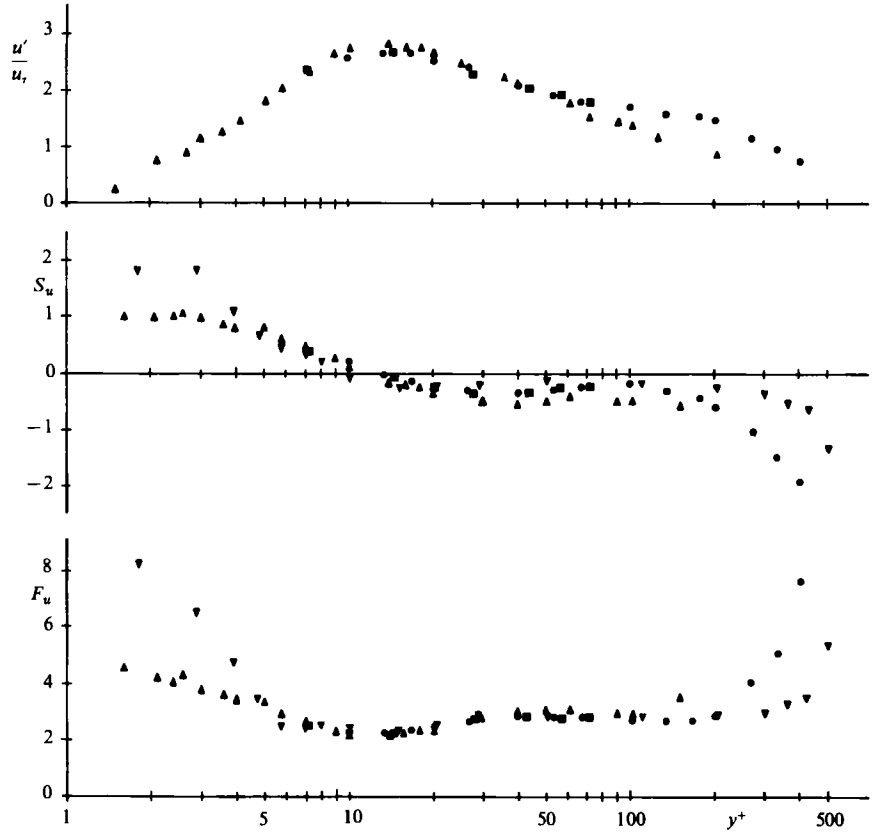

FIGURE 8. Logarithmic distribution of dimensionless moments of u-fluctuations in channel flow (Kreplin & Eckelmann based Re on centreline velocity and channel width). ●, $Re_\theta = 770$; ■, 730; ▼, 1900 (Gupta & Kaplan 1972); ▲, 7700 (Kreplin & Eckelmann 1979).

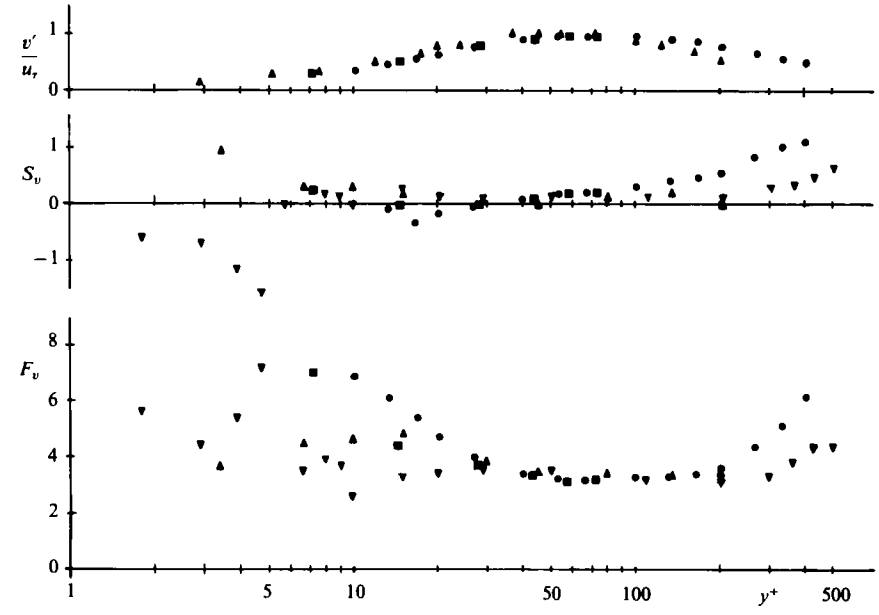

FIGURE 9. Logarithmic distribution of dimensionless moments of v-fluctuations in channel flow (see figure 8 for symbols).

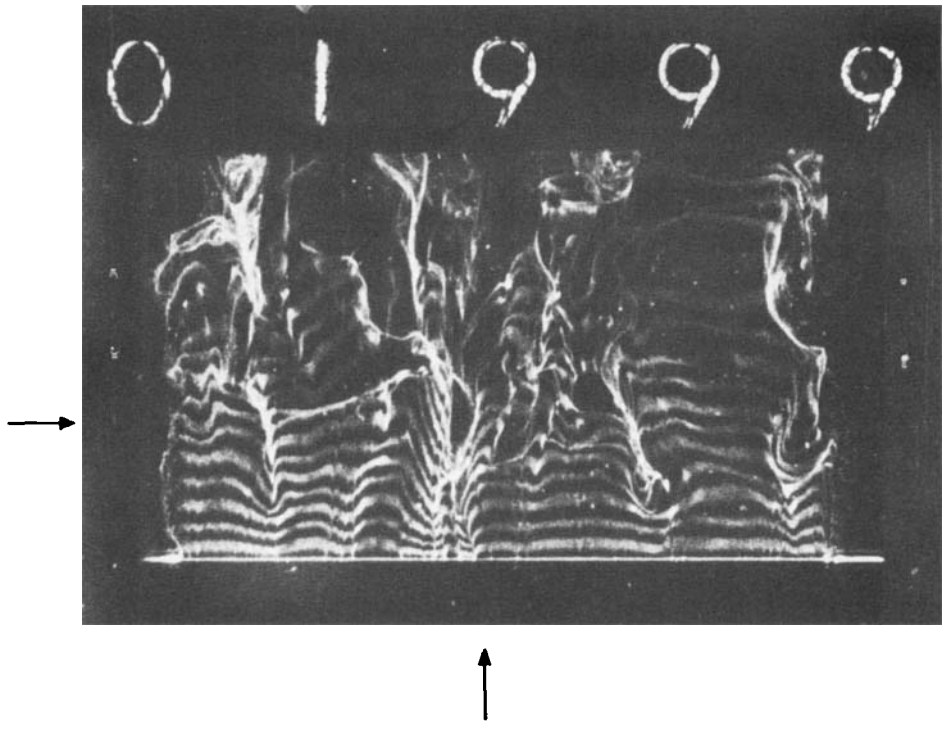

FIGURE 10. Low-speed and high-speed streaks in plan view. (Flow direction is from bottom to top. Intersection of arrows indicates dark spot.)

of the turbulent boundary layer owing to the difference in Reynolds number, but the results show the same tendency.

4. Observed flow structures

The films made in plan and in side view show a similar flow picture to that observed in the visualization studies of Kline and his colleagues at Stanford University (Runstadler, Kline & Reynolds 1963; Kline *et al.* 1967; Kim, Kline & Reynolds 1971; Offen & Kline 1973). Flow phenomena observed by others can also be seen on the frames (Corino & Brodkey 1969 – ejection; Falco 1977 – bulge and typical eddy; Head & Bandyopadhyay 1981 – horseshoe vortex). Of course, on a single photograph the shape of the bubble 'lines' gives no information about the instantaneous velocity field. The determination of the position and timing of an event requires measurements of the line movements between successive frames of the film. For the sake of completeness a short summary of our observations follows.

The most remarkable structures observed in plan view at $y^+ = 29$ (with velocity measurement at $y^+ = 14$) are the low-speed streaks, visible on the frames as areas of accumulation of hydrogen bubbles; areas long in the streamwise direction and short in the lateral direction (figure 10). These low-speed streaks are very persistent and are consistently longer than $490x^+$, the maximum distance visible on the frames in the streamwise direction. The width of the streaks ranges from $20z^+$ to $40z^+$. The intermittency of the low-speed streaks, their apparent disappearance and reappearance (Smith & Schwartz 1983), is also observed. The disappearance of a low-speed streak

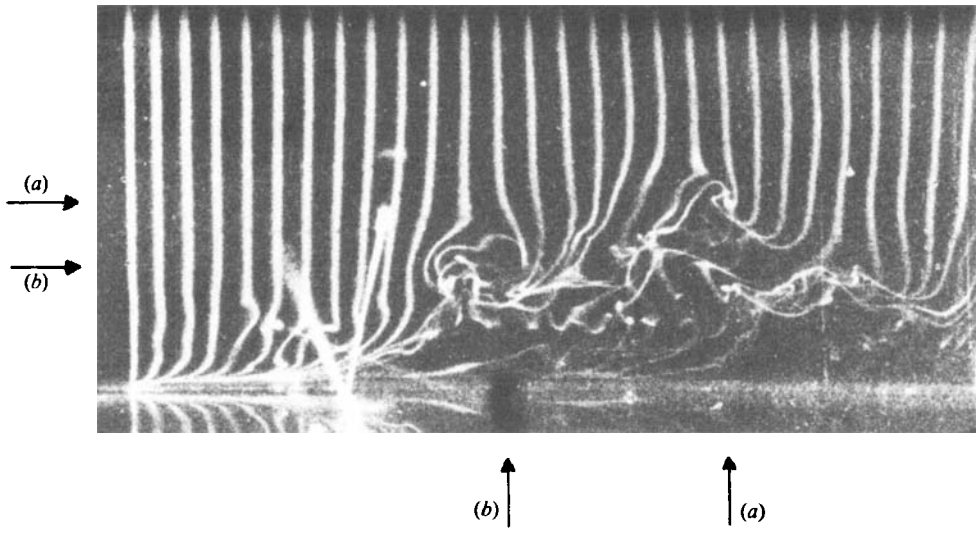

FIGURE 11. Side view of turbulent channel flow. (Flow direction is from left to right. Intersections of arrows indicate typical eddies.)

is frequently accompanied by a so-called dark spot. Just before disappearance a dark spot, which is a small area within a streak from which the hydrogen bubbles have disappeared, appears at the centreline of a streak (figure 10). It is believed that these dark spots are closely related to the ejection described by Corino & Brodkey (1969).

The low-speed streaks alternate with high-speed streaks (figure 10). In high-speed streaks the hydrogen-bubble concentration is low. The width of these streaks is two to four times the width of low-speed streaks and the high-speed streaks can also be longer than $490x^+$. The strongly vortical nature of a turbulent boundary layer is not revealed by the films made in plan view; only oscillation in the lateral direction is visible. On the films made with the platinum wire placed at $y^+ = 57$ (with measurements at $y^+ = 43$) the phenomena described above are also visible but, as expected, not so clear.

On looking at the films made in side view attention is drawn by the intermittency in the outer layer. Large-scale motions, bulges (Falco 1977, most probably type T1), are followed by large, nearly undisturbed, regions which can reach the wall region. The upstream interface between a bulge and a nearly undisturbed region is often quite sharp, making an angle of 15°–30° in the streamwise direction with the wall. At this interface, the back of the bulge, transverse eddies are visible of diameter of the order of $100y^+$. These eddies are called 'typical eddies' by Falco (1977); see figure 11. The presence of the laser beams makes it more difficult to study the motion in the wall layer in side view. As mentioned, nearly undisturbed regions can reach the wall region. Then small oscillations or even a solitary typical eddy can be found there. Close to the wall small longitudinal vortices are sometimes seen making an angle of 0°–10° in the streamwise direction with the wall. These vortices can be accompanied by a movement of hydrogen bubbles away from the wall, but this movement can also be perceived in the absence of these vortices. The movement of vortices away from the wall takes place beneath the back of the bulge. Kim *et al.* (1971) associated this bubble movement or the appearance of longitudinal vortices in the wall region with the ejection of a low-speed streak. Not only in the wall region but throughout the

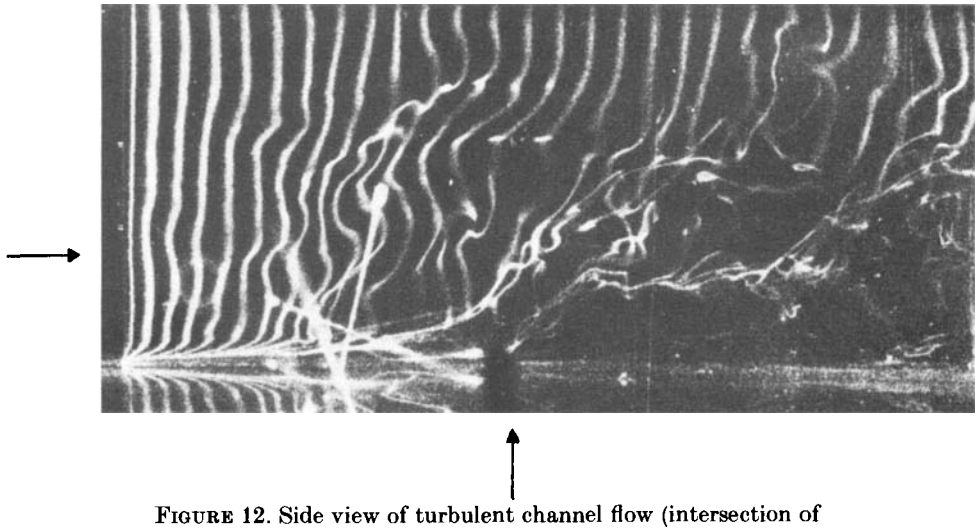

FIGURE 12. Side view of turbulent channel flow (intersection of arrows indicates horseshoe vortex).

whole boundary layer longitudinal vortices can be observed. These vortices make an angle of 0°–45° with the wall in the downstream direction. The diameter of these vortices ranges from 10 to 50 y^+. Sometimes the arrangement of vortices is such that they can be part of a horseshoe vortex (figure 12).

5. Relation between observed flow structures and Reynolds stress

5.1. *Characteristic signals of flow structures in the wall layer*

Using a film viewer and a graphics terminal it is possible to study the filmed structures in the neighbourhood of the measuring point together with the simultaneously measured signals. In spite of interpretation problems due to the three-dimensional, time-dependent character of the flow there seem to be signals characteristic of low- and high-speed streaks. Since plan-view visualization and measurement were not performed at exactly the same wall distance, the correlation of observed structures and measured signals is weakened. Where a structure is present at the measuring point as well as in the visualized area above that point there is no interpretation problem. But, if a structure is so small, i.e. owing to intermittency of a low-speed streak, or if a structure is found in such an oblique position in the flow that it is present either in the visualized area alone or at the measuring point alone, there will be no correlation between image and signals. In side view, visualized area and measuring point need not necessarily have the same lateral position, because the hydrogen bubbles are also moving in a lateral direction. This causes interpretation problems too which will be attributed in the discussion below to this spatial separation between visualized area and measuring point.

5.1.1. *Low-speed streaks*

When in plan view a low-speed streak is perceived above the measuring position, the measured velocity component in the streamwise direction correlates well – the value – and the normal velocity is positive. So a low-speed streak is moving away instantaneous streamwise velocity component is lower than its time-averaged

from the wall and is slower than the average flow in the streamwise direction. This implies a positive contribution to the Reynolds stress. This contribution is not constant but very intermittent owing to oscillation and disappearance and reappearance of the streaks. If the measuring point is found for some time in a low-speed streak, the streak contributes continuously to the Reynolds stress. In dark spots larger contributions to the Reynolds stress are measured.

The characteristic signals of a low-speed streak, negative u-component ($u \leqslant -2u_\tau$) and positive v-component, are also observed in the signals measured during filming in side view. But the correlation between image and signals is quite obscure. Low-speed streaks are not often marked by the hydrogen bubbles in side-view films, because the streaks are not wide enough. As these streaks also move in a lateral direction, the probability that measurement will take place within a marked low-speed streak, is not high. Sometimes it is observed that a low-speed streak is moving away from the wall. If measurement is performed on such a streak, the streak is seen to make a substantial contribution to the Reynolds stress. More quantitative details follow. We believe that significant contributions to the Reynolds stress are asociated with bursts and ejections in low-speed streaks. Bogard (1982) draws a similar conclusion, based on an investigation of dye motions and simultaneously measured uv-signals.

5.1.2. *High-speed streaks*

Observation and measurement of high-speed streaks correlate well in both plan and side view. With a high-speed streak the measured streamwise velocity is for some time greater than the mean velocity and frequently the normal velocity is slightly negative. This negative v-component is measured in particular in high-speed streaks appearing immediately after bulges. So a high-speed streak is moving faster in the streamwise direction than the mean flow and the streak is often moving slowly towards the wall. In both low- and high-speed streaks high contributions to the Reynolds stress are measured. But, in contrast to the low-speed streaks, in high-speed streaks no phenomena are observed which can account for these contributions. This may be caused by the stationary position of the camera: probably films made with a moving camera would reveal more details of high-speed streaks. Contributions to the Reynolds stress by high-speed streaks take place in the fourth quadrant of the (u, v)-plane. Contributions in this quadrant are usually attributed to the sweep (Lu & Willmarth 1973; Brodkey, Wallace & Eckelmann 1974), but from our investigation it is not clear which part of the sweep is responsible.

5.1.3. *Eddies*

Longitudinal and transverse (typical?) eddies are observed in the wall region and both are accompanied by high contributions to the Reynolds stress. For the typical eddies this is in agreement with Falco's (1977) measurements, but no characteristic signals are observed during the passage of longitudinal or typical eddies. The contributions to the Reynolds stress do not take place in a particular quadrant, probably because the measurements are not performed at the same points in these eddies. Owing to different spatial separation between eddies and measuring point the measurements will be carried out each time in different parts of the eddies.

5.1.4. *Some illustrations*

In figures 13 and 14 examples are given on which the above discussion has been based. Some frames of a film made in plan view, and the corresponding u-, v- and

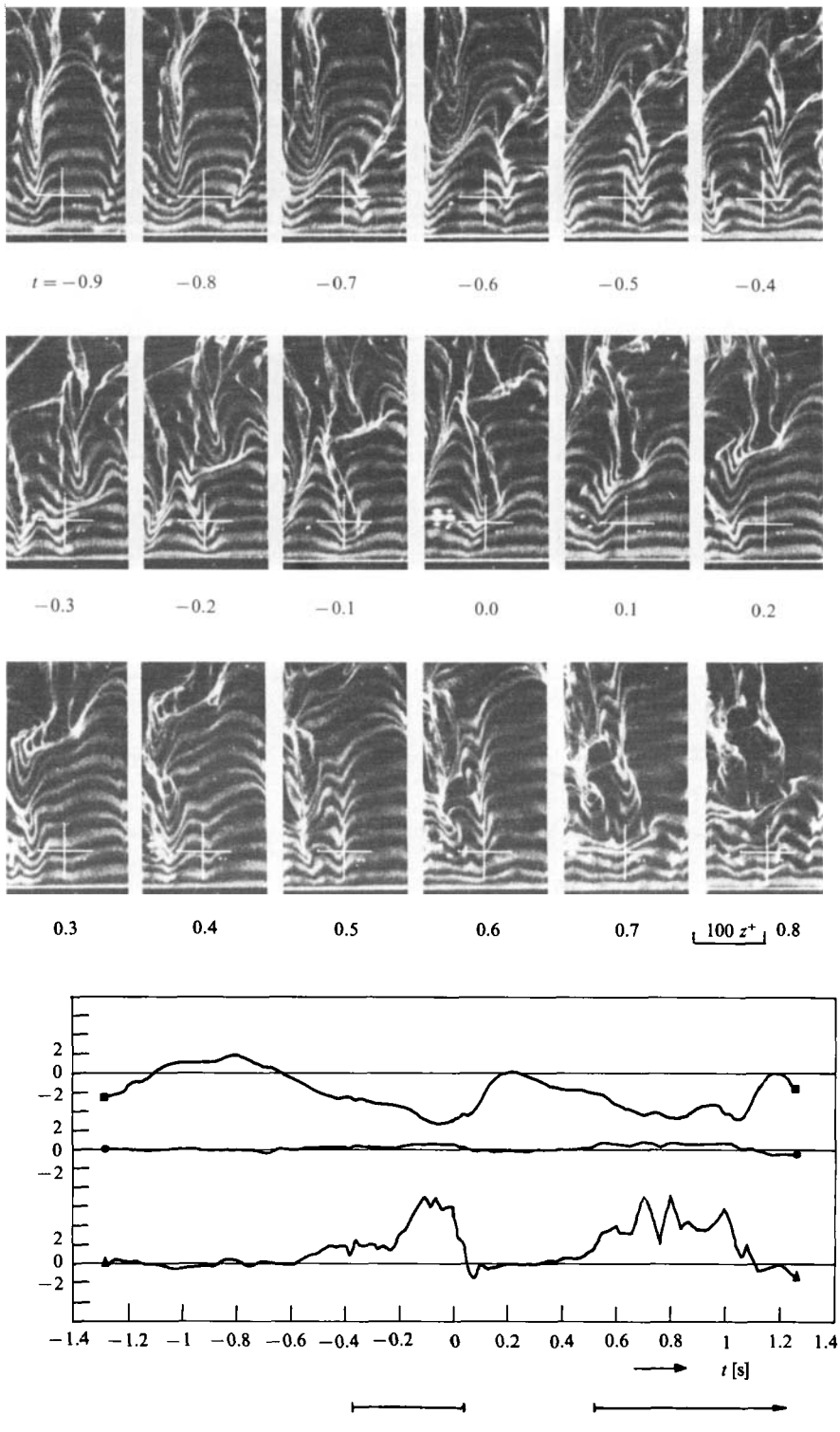

FIGURE 13. Measurement and visualization in plan view. Solid bars beneath the velocity signals indicate coherent *uv*-groups. ■, u/u_τ; ●, v/u_τ; ▲, $uv/\overline{uv}$.

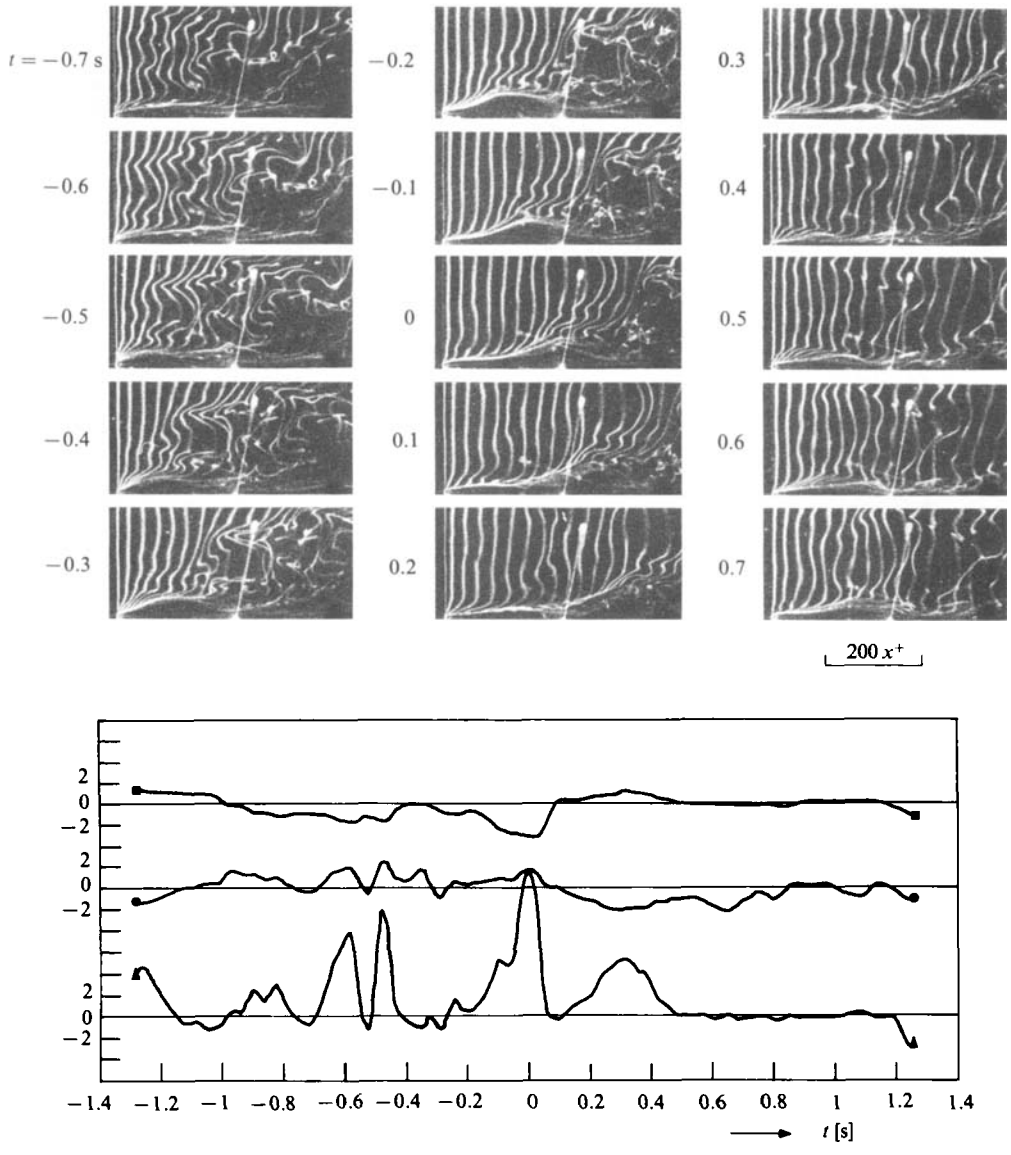

FIGURE 14. Measurement and visualization in side view. Symbols as in figure 13.

uv-parts are shown in figure 13. The frames are not reproduced entirely, but only the area around the measuring point (dimensions 380 $x^+ \times 190$ z^+). The flow direction on the pictures is from bottom to top. At the bottom of the pictures the platinum wire generating hydrogen bubbles is visible. The measuring point is marked on each picture with a plus sign. The non-dimensional signals are plotted against a time axis from which the origin has been translated. The origin of the axis corresponds to frame number 1420 of the film. Beneath each picture the corresponding time is given. On the pictures indicated with $t = -0.9$ to 0.2 s a low-speed streak is moving towards the measuring point and replacing a high-speed streak. During this time interval a decrease is observed in the u-signal and an increase in the v-signal. At $t = -0.1$ s a

dark spot appears. In the corresponding uv-signal a peak is observed (second quadrant; $uv/\overline{uv} = 7$). Immediately afterwards the low-speed streak is pushed away by a high-speed streak. At $t = 0.5$ s a low-speed streak is again perceived. On the following pictures the flow is quite disorderly, while the signals indicate that measurement is still performed in a low-speed streak which makes a high contribution to the Reynolds stress. This is probably caused by intermittency of the streak.

In figure 14 some pictures of a film made in side view and the corresponding parts of the measured signals are shown. Again the frames are not reproduced entirely; the dimensions of a picture are 580 $x^+ \times 250$ y^+. The flow direction is from left to right. On the left of the picture the platinum wire is visible. The intersecting laser beams mark the measuring position. The origin of the time-axis of the plotted signals corresponds now with the frame number 12205 of the film. On the left of each picture the corresponding time is given. On the pictures marked with $t = -0.7$ to 0 s the formation of a typical eddy is visible above and downstream of the measuring point. At $y^+ = 43$ a low-speed streak is measured contributing to the Reynolds stress in the second quadrant. The contributions at about $t = -0.6$ and -0.5 s cannot be connected with any visible flow structure. At $t = 0$ s the movement away from the wall gives the contribution. Upstream of the measuring point a high-speed streak appears which sweeps away the low-speed streak. From the high-speed streak a contribution to the Reynolds stress is measured at $t = 0.3$ s in the fourth quadrant. On the following pictures not much turbulence is observed and simultaneously components are measured at almost the mean velocity. More illustrations can be found in Talmon (1984).

5.2. *Contributions to second quadrant of uv-plane*

As shown earlier a connection exists between observed low-speed streaks and measured high contributions to the Reynolds stress taking place in the second quadrant of the uv-plane. Especially in plan view the occurrence of low-speed streaks is accompanied by contributions to the Reynolds stress in quadrant 2. In side view this connection is not so obvious owing to spatial separation. It has been found earlier that, applying the quadrant-analysis technique to signals measured in the turbulent wall region, the second and fourth quadrants of the (u, v)-plane provide in a short time the major part of the Reynolds stress (Lu & Willmarth 1973; Brodkey *et al.* 1974). As can be seen in figure 15 this applies also to signals measured during and after filming in our turbulent channel flow. In figure 15 $(\overline{uv})_i/\overline{uv}$ and t_i/t ($i = 2$, 4 or 5) calculated for the 78 s and 30 min signals of a film made in plan view (measured at $y^+ = 14$) are plotted as functions of hole-size K ($|uv| = K|\overline{uv}|$). $(\overline{uv})_i$ represents the average value of uv for quadrant 2 ($i = 2$), quadrant 4 ($i = 4$) or the hole ($i = 5$); $\overline{uv}$ is the average value for $i = 1$–5. t_i is the time of the uv-signal in quadrant 2 ($i = 2$), quadrant 4 ($i = 4$) or the hole ($i = 5$); t is the total time. In the case of the 78 s signal the Reynolds stress averaged over 30 min is used in the calculation of the hole magnitude. The difference between the 78 s and 30 min signals will be due to the short averaging time of the 78 s signal.

Studying the individual contributions in the second quadrant of a film made in plan view, it appears that almost every contribution of magnitude $K|\overline{uv}|$ with $K \geqslant 2$ is caused by a low-speed streak (about 90%). Due to spatial separation, when measuring at $y^+ = 14$ and filming at $y^+ = 29$ sometimes a contribution can be found without a visible low-speed streak. With $K = 2$ also not every visible streak is detected; a few streaks are not strong enough to cause a detection at the measuring time. Intermittency and oscillation of low-speed streaks is observed. Hence more than

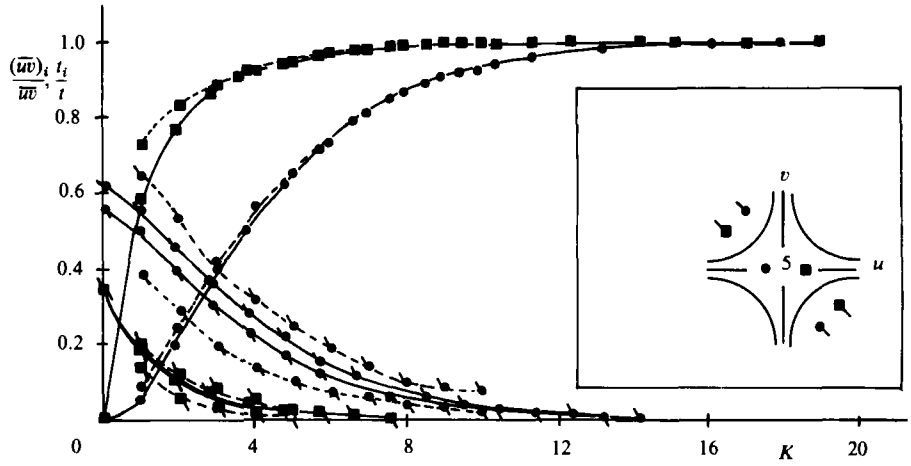

FIGURE 15. Fractional contribution to Reynolds stress and time fraction as function of hole-size $K = |uv/\overline{uv}|$ of signals measured during and after filming (quadrant analysis technique). – – – –, 78s; ——, 30 min; ●, $(\overline{uv})_i/\overline{uv}$; ■, t_i/t.

one contribution can be found originating from the same low-speed streak. About half of the low-speed streaks have more than one contribution with an absolute magnitude greater than or equal to $2|\overline{uv}|$; on average two such contributions are measured for low-speed streaks.

Assuming that these contributions (frequently coinciding with dark spots) are closely related to ejections and bursts, coherent structures can be detected and counted in the second quadrant of the (u, v)-plane with $|uv| \geqslant 2|\overline{uv}|$. The distribution of time intervals t_d between successive detections by this method of detection has been calculated. t_d is defined as the time interval between the middle of the first and the middle of the second detection. For two films (total duration of signals 171 s) this distribution is shown in figure 16. The mean time T_d between successive detection is 0.82 s for these films.

From them it was observed that on average two contributions are made to the Reynolds stress in quadrant 2 by each low-speed streak. Offen & Kline (1973) perceived two ejections per burst. They assumed that dye activities (ejections) with time intervals smaller than a threshold level τ_d belong to the same burst. Here a similar assumption is made. Based on hydrogen-bubble observations it is assumed that detections at $y^+ = 14$ with time intervals smaller than 0.42 s are detections of the same structure. Most probably this structure is a burst, but for the time being this structure is called a coherent uv-group. The visual classification of detections arising from the same low-speed streak agrees very well with the numerical classification of detections belonging to one coherent uv-group.

In figure 13 the relation between uv-group detections and visual observations is illustrated. The first group consists of 5 contributions $> 2|\overline{uv}|$. The second uv-group is part of a larger uv-group (extending to $t = 2.3$ s); the part shown in figure 13 consists of three contributions $> 2|\overline{uv}|$. In both cases the uv-group is closely associated with one low-speed streak. In figure 17 the distribution of time intervals t_g between successive coherent uv-groups is shown. The time interval t_g is defined in the same way as time interval t_d. To calculate the distribution the signals of three films (total duration 268 s) were used. The mean time T_g between successive coherent uv-groups is 2.1 s.

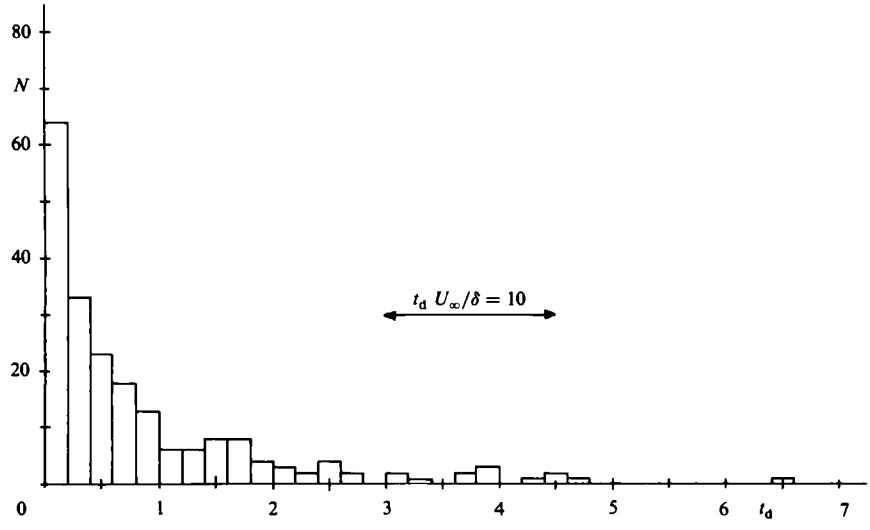

FIGURE 16. Distribution of time intervals between successive detections according to the second-quadrant analysis. $T_d = 0.82$ s.

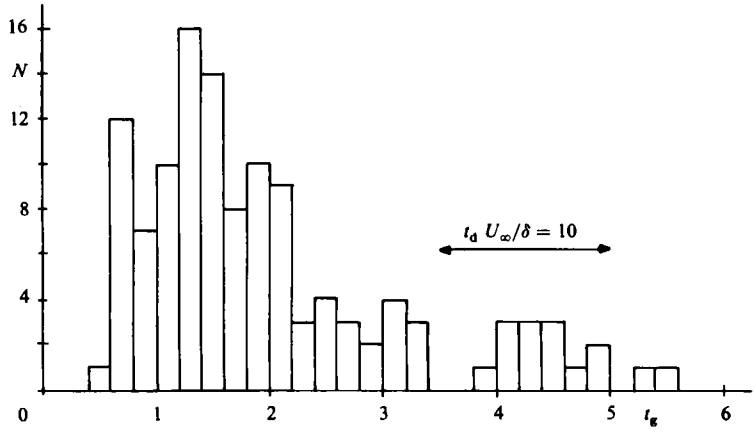

FIGURE 17. Distribution of time intervals between successive coherent uv-groups. $T_g = 2.1$ s.

Our study was carried out independently of that of Bogard (1982). Based on dye observations and hot-film measurements Bogard designed a detection method for coherent structures similar to our method mentioned above. With his method, detection of ejections was assumed to occur when the instantaneous uv-signal is found in the second quadrant and when the following relation holds: $|uv| \geqslant Hu'v'$. In a water flow ($U_\infty = 14.6$ cm/s, $\theta = 0.27$ cm, $u_\tau = 0.79$ cm/s) Bogard measured a value of 1.1 s for the mean time between successive detections ($y^+ = 15$; signal duration 200 s; $H = 1.07$). Bogard assumed that two successive ejections, detected with $H = 1.07$, belong to one burst if the time interval is smaller than 0.8 s. He found in that way a mean time between successive bursts of 2.2 s. These bursts were responsible for 80% of the contribution of the complete second quadrant to the Reynolds stress. Bogard used for hole size H the value 1.07, the ratio of the Reynolds stress of the second quadrant (averaged over the time the uv-signal spent in the second quadrant) and the Reynolds stress of the complete signal, because Comte-Bellot,

K	N	T_g (s)	$\overline{uv_g}/\overline{uv}$ (%)	$\Delta t_g/t$ (%)
2	33	2.4	55	19
3	26	3.0	47	13
4	20	3.9	35	7
5	14	5.6	29	5

TABLE 2. Some results of the second-quadrant analysis technique, $K = 2$–5

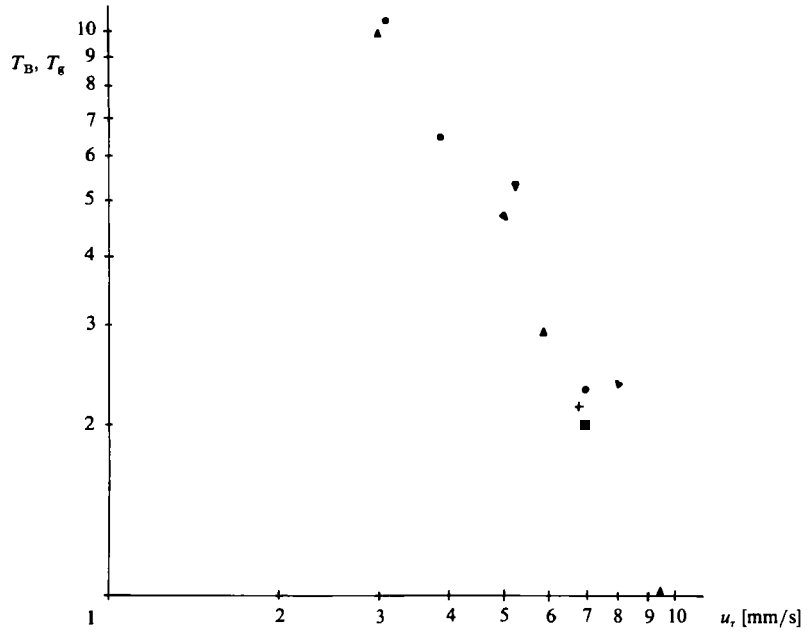

FIGURE 18. Mean period of bursts and coherent uv-groups. ▲, Runstadler *et al.* (1963); ■, Schraub & Kline (1965); ●, Kim *et al.* (1971); ▼, Offen & Kline (1973); ▼, Smith (1978); ◀, Bogard (1982); +, channel flow.

Sabot & Saleh (1979) found that ratio to be nearly constant in the core region of a fully developed turbulent pipe flow. The hole-size Bogard used is, in our second-quadrant analysis, comparable with $K = 3$. In table 2 quantities calculated for coherent uv-groups detected with K-values of 2–5 are given. In this table N represents the number of detected uv-groups, $-\rho\overline{uv}_g$ the Reynolds stress due to the coherent uv-groups and Δt_g is the total time coherent uv-groups are detected. If $K = 3$, 47 % of the Reynolds stress is contributed by coherent uv-groups in 13 % of the time. This corresponds to 75 % of the Reynolds stress due to the second quadrant. In spite of the good agreement between Bogard's and our results one should keep in mind that both of these studies are based on short signals, so the uncertainty in the results is quite large.

In figure 18 the mean time T_g between successive coherent uv-groups ($K = 2$, $\tau_d = 0.42$ s) and the mean time T_B between successive bursts (detected visually by other investigators) are compared in dimensional form, T_B (T_g) *versus* u_τ, resulting in a very good agreement.

The distribution of time intervals between successive detections as given in figure 16

does not resemble the distribution found by Kim *et al.* (1971), because our detections as given in figure 16 are probably ejections and the structures observed by Kim *et al.* are bursts. On introducing the coherent *uv*-groups the distribution of time intervals, as given in figure 17, attains the same form as the distribution of Kim *et al.* Thus it is likely that our coherent *uv*-groups are identical with the visual bursts as defined by the Stanford group.

6. Conclusion and discussion

The measurement of two velocity components, using a laser-Doppler anemometer, and hydrogen-bubble flow visualization were combined in a turbulent boundary layer of a channel flow. Not only were the same flow phenomena perceived on the films of the water flow as observed by Runstadler *et al.* (1963), Kline *et al.* (1967), Kim *et al.* (1971) and Offen & Kline (1973), but also other phenomena appeared to be visible, viz the ejection (Corino & Brodkey 1969), the bulge and the typical eddy (Falco 1977) and the horseshoe vortex (Head & Bandyopadhyay 1981).

Owing to the three-dimensional, time-dependent character of the flow it was rather difficult to identify flow structures from measured velocity signals, especially at larger distances from the wall. However, in the wall region such an identification was possible. The quadrant-analysis technique was adopted for the detection of structures in the wall region, using only *uv*-parts of the second quadrant with an absolute magnitude greater than or equal to $2|\overline{uv}|$. In this way a high correlation was achieved between visual and measured detections of ejections. Assuming that measured detections with time intervals smaller than 0.42 s are detections of the same structure – this assumption is based on visual observations – the visual observed burst is detected. In this way the three-dimensional and time-dependent character of the flow is taken into account.

Results of this method of detection are not quite free from subjectivity, but it seems quite certain that coherent structures are detected. With the second-quadrant detection method it will be possible to investigate the properties of coherent structures quite accurately. The information on coherent structures can then be used for modelling turbulent flows. But first the same experiments should be carried out at higher Reynolds numbers, because the properties of coherent structures may change with Reynolds number; see for instance Head & Bandyopadhyay (1981).

REFERENCES

BOGARD, D. G. 1982 Investigation of burst structures in turbulent channel flows through simultaneous flow visualization and velocity measurements. Thesis, Purdue University.

BRODKEY, R. S., WALLACE, J. M. & ECKELMANN, H. 1974 Some properties of truncated signals in boundary shear flows. *J. Fluid Mech.* **63**, 209.

CLAUSER, F. H. 1956 The turbulent boundary layer. *Adv. Appl. Mech.* **4**, 1.

COMTE-BELLOT, G., SABOT, J. & SALEH, I. 1979 Detection of intermittent events maintaining Reynolds stress. In *Proc. Dynamic Flow Conf. 1978*. The Netherlands: Sijthoff and Noordhoff.

CORINO, E. R. & BRODKEY, R. S. 1969 A visual investigation of the wall region in turbulent flow. *J. Fluid Mech.* **37**, 1.

FALCO, R. E. 1977 Coherent motions in the outer region of turbulent boundary layers. *Phys. Fluids* **20**, S124.

GUPTA, A. K. & KAPLAN, R. E. 1972 Statistical characteristics of Reynolds stress in a turbulent boundary layer. *Phys. Fluids* **15**, 981.

HEAD, M. R. & BANDYOPADHYAY, P. R. 1981 New aspects of turbulent boundary layer structure. *J. Fluid Mech.* **107**, 297.

HINZE, J. O. 1975 *Turbulence* 2nd edn. McGraw-Hill.

KIM, H. T., KLINE, S. J. & REYNOLDS, W. C. 1971 The production of turbulence near a smooth wall in a turbulent boundary layer. *J. Fluid Mech.* **50**, 133.

KLINE, S. J., REYNOLDS, W. C., SCHRAUB, F. A. & RUNSTADLER, P. W. 1967 The structure of turbulent boundary layers. *J. Fluid Mech.* **30**, 741.

KREPLIN, H.-P. & ECKELMANN, H. 1979 Behaviour of the three fluctuating velocity components in the wall region of a turbulent channel flow. *Phys. Fluids* **22**, 1233.

KUNEN, J. M. G. 1984 On the detection of coherent structures in turbulent flows. Doctoral Dissertation, Delft University of Technology, Delft, The Netherlands.

LU, S. S. & WILLMARTH, W. W. 1973 Measurements of the structure of the Reynolds stress in a turbulent boundary layer. *J. Fluid Mech.* **60**, 481.

OFFEN, G. R. & KLINE, S. J. 1973 Experiments on the velocity characteristics of 'bursts' and on the interaction between the inner and outer regions of a turbulent boundary layer. *Rep. no.* MD-31, Stanford University, Stanford, California.

RUNSTADLER, P. W., KLINE, S. J. & REYNOLDS, W. C. 1963 An investigation of the flow structure of the turbulent boundary layer. *Rep. no.* MD-8, Stanford University, Stanford, California.

SCHRAUB, F. A. & KLINE, S. J. 1965 A study of the structure of the turbulent boundary layer with and without longitudinal pressure gradient. *Rep. no.* MD-12, Stanford University, Stanford, California.

SMITH, C. R. 1978 Visualization of turbulent boundary layer structure using a moving hydrogen bubble probe. In *Proc. of the Workshop on Coherent Structure of Turbulent Boundary Layer, Lehigh University, Bethelehem, Pennsylvania.*

SMITH, C. R. & SCHWARTZ, S. P. 1983 Observation of streamwise rotation in the near-wall region of a turbulent boundary layer. *Phys. Fluids* **26**, 641.

TALMON, A. M. 1984 Simultane visualisatie-studie en snelheidsmetingen aan coherente structuren in een turbulente grenslaag. *Internal report Delft University of Technology, Delft, The Netherlands.*